Flow Instabilities in Cavitating and Non-Cavitating Pumps

Yoshinobu Tsujimoto
Engineering Science, Osaka University
1-3 Machikaneyama, Toyonaka
Osaka, 560-8531
JAPAN

tujimoto@me.es.osaka-u.ac.jp

ABSTRACT

It is well known that flow instabilities called rotating stall and surge may occur in non-cavitating turbomachines at flow rates smaller than design. Rotating stall is a local instability at the turbomachinery which is basically not dependent on the hydraulic system in which the turbomachine is installed. The stalled region rotates faster than impeller. Surge is a system instability in a hydraulic system which includes a turbomachinery and a capacitance (tank) which stores the working fluid depending on the pressure at the capacitance. For pumps, if a certain quantity of air is trapped in the pipeline it serves as a capacitance and a surge may occur even if the pipeline does not include exernalt capacitance. Both rotating stall and surge occur at smaller flow rates where the performance curve has a positive slope.

On the other hand, cavitation instabilities called rotating cavitation and cavitation surge may occur even at the design flow rate. Rotating cavitation is a local instability in which the cavitated region rotates, for the most cases, faster than impeller. Cavitation surge is a system instability caused by cavitation. For cavitation surge, the cavitation at the inlet of turbomachinery serves as a capacitance and it can occur in a system without any external capacitance.

The present lecture is intended to explain the mechanisms of the instabilities, rotating stall, surge, rotating cavitation, and cavitation surge, as well as the characteristics of those instabilities, based on one [1] and two [13][14] dimensional stability analyses.

1.0 IMPELLER PERFORMANCE AND CAVITATION CHARACTERISTICS

To be used for a one dimensional stability analysis of the instabilities, the impeller performance and the cavitation characteristics are modelized in this section.

1.1 Impeller Performance

We consider a cascade as shown in Fig.1, rotating with the velocity of U_T in a uniform axial velocity of U. The blade spacing h is assumed to be sufficiently small as compared with the blade length l and the flow in the cascade is perfectly guided by the blades. The axial and tangential velocity disturbances are represented by δu_1 and δv_1, respectively, at the inlet, and the axial velocity disturbance δu_2 at the outlet. The cavity of volume V_c per blade appears at the inlet. The velocity triangle at the inlet is shown in Fig.1.

Tsujimoto, Y. (2006) Flow Instabilities in Cavitating and Non-Cavitating Pumps. In *Design and Analysis of High Speed Pumps* (pp. 7-1 – 7-24). Educational Notes RTO-EN-AVT-143, Paper 7. Neuilly-sur-Seine, France: RTO. Available from: http://www.rto.nato.int/abstracts.asp.

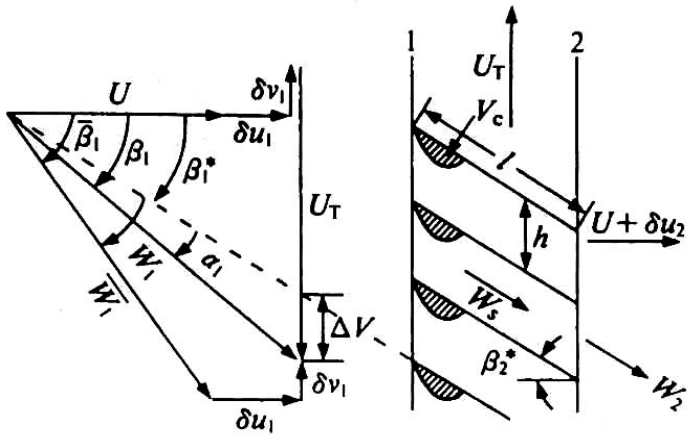

Figure 1: Rotor Cascade and Inlet Velocity Triangle.

It is assumed that all of the cavitation can be lumped into the volume V_c, upstream of the blade passage, and that the subsequent rotor flow can be modeled as single-phase incompressible liquid flow (the more complex blade passage model of Brennen [2] suggests that this is a good first approximation). Then the unsteady Bernoulli's equation applied to the relative flow in the rotor yields

$$\frac{p_2 - p_1}{\rho} = \frac{1}{2}(W_1^2 - W_2^2) - \frac{\partial *}{\partial t *}(\phi_2 - \phi_1) - \frac{\Delta p_t}{\rho} \tag{1}$$

Here,

$$\frac{\partial *}{\partial t *} = \frac{\partial}{\partial t} + U_T \frac{\partial}{\partial y}$$

is a time derivative in a frame rotating with the rotor. If $\beta *$ is the average blade angle, as shown in Fig.1, the difference of the velocity potential can be approximated by

$$\phi_2 - \phi_1 = \int_1^2 W_s \, ds \cong \frac{u_2 l}{\cos \beta *}$$

The total pressure loss Δp_t in the impeller is represented by two coefficients, ζ_Q and ζ_S:

$$\Delta p_t / \rho = \zeta_Q (U + \delta u_1)^2 + \zeta_S (\Delta V)^2 \tag{2}$$

where ΔV is the incidence velocity as shown in Fig.1 and can be expressed as

$$\Delta V = (U + \delta u_1)(\tan \bar{\beta}_1 - \tan \beta_1 *)$$

Thus, ζ_Q represents the hydraulic loss in the blade passage, and ζ_S the incidence loss at the inlet. The differences between pressure fluctuations upstream and downstream of the impeller are obtained by considering Eqs.(1) and (2) after linearization to yield

$$\frac{\delta p_2 - \delta p_1}{\rho U^2} = (1 - L_u)\frac{\delta u_1}{U} - (\tan \bar{\beta}_1 + L_v)\frac{\delta v_1}{U} - \frac{1}{\cos^2 \beta_2 *}\frac{\delta u_2}{U} - \frac{1}{\cos \beta *}\frac{l}{U}\frac{\partial *}{\partial t *}\left(\frac{\delta u_2}{U}\right) \tag{3}$$

where L_u and L_v are given by

$$L_u = \frac{\partial \Delta p_t}{\partial(\rho U u_1)} = 2\zeta_Q + 2\zeta_S \tan\beta_1 * (\tan\beta_1 * - \tan\bar{\beta}_1)$$

$$L_v = \frac{\partial \Delta p_t}{\partial(\rho U v_1)} = 2\zeta_S (\tan\beta_1 * - \tan\bar{\beta}_1)$$

In general, cavitation instabilities appear at larger cavitation number than those which brings about significant deterioration in the pressure performance. Therefore, the effect of cavitation on the pressure rise across the rotor has been omitted from the present analysis and is not included in Eq.(3).

1.2 Cavitation

The cavity volume V_c per blade and per unit span is normalized using the blade spacing h and represented by a.

$$a(\sigma\ ,\alpha_1) \equiv V_c/(h^2 \times 1) \tag{4}$$

Under quasi-steady conditions, the non-dimensional cavity volume a is considered to be a function of the incident angle α_1 and the inlet cavitation number σ defined as follows.

$$\sigma = \frac{p_1 - p_v}{\rho W_1^2/2} \tag{5}$$

where p_1, p_v and W_1 are the inlet pressure, the vapor pressure, and the inlet relative velocity, respectively. Then, as originally suggested by Brennen and Acosta [3], the change of cavity volume, δV_c, is related to the deviations $\delta W_1, \delta p_1$, and $\delta\alpha_1$ by

$$\delta V_c = h^2\left[\frac{\partial a}{\partial\sigma}\left(\frac{\partial\sigma}{\partial W_1}\delta W_1 + \frac{\partial\sigma}{\partial p_1}\delta p_1\right) + \left(\frac{\partial a}{\partial\alpha_1}\right)\delta\alpha_1\right] \tag{6}$$

From the velocity triangle shown in Fig.1, the deviations δW_1 and $\delta\alpha_1$ can be represented in terms of the deviations δu_1 and δv_1 from the uniform axial velocity. Then Eq.(6) may be written as

$$\delta V_c = h^2\left[F_1\cdot\left(\frac{\delta u_1}{U}\right) + F_2\cdot\left(\frac{\delta v_1}{U}\right) + F_3\cdot\left(\frac{\delta p_1}{\rho U^2}\right)\right] \tag{7}$$

where

$$F_1 = 2\sigma K\cos^2\bar{\beta}_1 - M\sin\bar{\beta}_1\cos\bar{\beta}_1,$$

$$F_2 = -2\sigma K\sin\bar{\beta}_1\cos\bar{\beta}_1 - M\cos^2\bar{\beta}_1, \quad F_3 = -2K\cos^2\bar{\beta}_1 \tag{7'}$$

and

$$M = \frac{\partial a}{\partial\alpha_1}, \quad K = -\frac{\partial a}{\partial\sigma}. \tag{8}$$

M and K are the mass flow gain factor and cavitation compliance, respectively. For the evaluation of these factors, see Brennen [4], Ng and Brennen [5], and Otsuka et al.[6].

The continuity relation across the impeller is

$$h(\delta u_2 - \delta u_1) = (\partial * / \partial t*)\delta V_c \tag{9}$$

where subscripts 1 and 2 indicate the inlet and outlet of the impeller.

By combining Eqs.(7) and (9), the continuity equation can be expressed as follows:

$$\delta u_2 - \delta u_1 = h(\partial * / \partial t *)\left[F_1 \cdot (\frac{\delta u_1}{U}) + F_2 \cdot (\frac{\delta v_1}{U}) + F_3 \cdot (\frac{\delta p_1}{\rho U^2}) \right] \tag{10}$$

2.0 SURGE

For surge, we consider a system composed of an inlet pipe with the length L and the cross sectional area f, a rotor shown in Fig.1, a surge tank with the surface area A, and the discharge valve with the cross sectional area f, as shown in Fig.2. The inlet pipe is connected to a large space with a constant pressure. By applying unsteady Bernoulli equation to the inlet pipe, we can evaluate the pressure disturbance at the rotor inlet:

$$\delta p_1 = -\rho U \delta u_1 - \rho L (d / dt) \delta u_1 \tag{11}$$

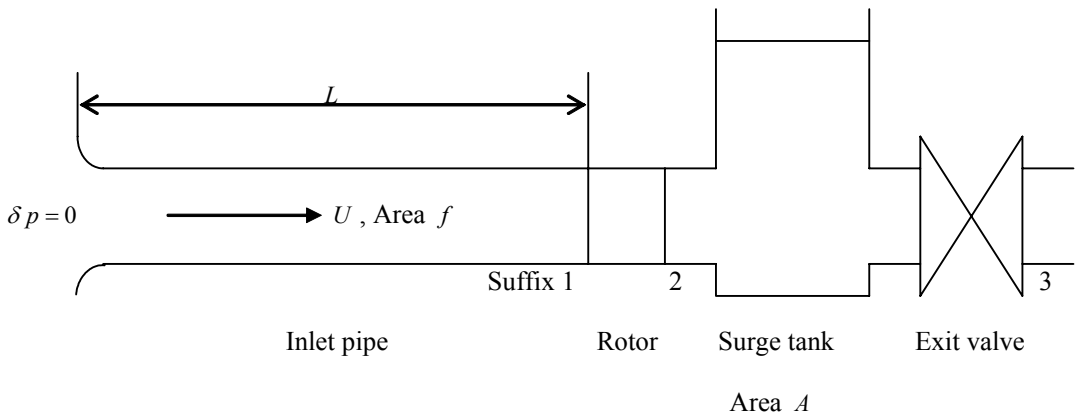

Figure 2: Hydraulic System for Surge Analysis.

For surge, we assume no cavitation at the inlet and the continuity relation across the rotor is,

$$\delta u_2 - \delta u_1 = 0 \tag{12}$$

Only axial flow disturbance occurs for surge and hence $\delta v_1 = 0$. Then, the pressure increase across the rotor, Eq.(3) , is reduced to:

$$\frac{\delta p_2 - \delta p_1}{\rho U^2} = (1 - L_u - \frac{1}{\cos^2 \beta_2 *})\frac{\delta u_1}{U} - \frac{1}{\cos \beta *}\frac{l}{U}\frac{d}{dt}(\frac{\delta u_1}{U}) \tag{13}$$

The continuity equation across the surge tank can be written as:

$$\delta u_2 - \delta u_3 = (A/\rho g f)(d\,\delta p_2/dt) = C(d\,\delta p_2/dt) \tag{14}$$

where g is the gravitational acceleration constant and $C = A/\rho g f$ is the compliance of the tank. The valve downstream of the tank discharges the flow into a contant pressure region and has the following characteristics:

$$\delta p_2/\rho U^2 = R(\delta u_3/U) \tag{15}$$

The unknowns in the above formulation are $\delta u_1, \delta p_1, \delta u_2, \delta p_2, \delta u_3$ and Eqs(11)-(15) are used to obtain the following differential equation for δu_1. Completely the same differential equation is obtained for other unknowns.

$$\left[1+\frac{1}{\cos^2\beta_2*}\frac{l}{L}\right]B^2\phi^2\frac{d^2}{dt^2}\left(\frac{\delta u_1}{U}\right)+\left[\frac{1+(1/\cos\beta_2*)(l/L)}{R}+B^2\phi^2(L_u+\frac{1}{\cos^2\beta_2*})\right]\frac{d}{dt}\left(\frac{\delta u_1}{U}\right)$$

$$+\left[1+\frac{L_u+1/\cos^2\beta_2*}{R}\right]\left(\frac{\delta u_1}{U}\right)=0 \tag{16}$$

where

$$B=\sqrt{\rho C/L}\,U_T \tag{17}$$

is Greitzer's B factor [7],[8] and $\phi = U/U_T = \tan\bar{\beta}_1$ is the mean flow coefficient. Here we define the inlet total to outlet static pressure coefficient of the impeller $\psi_{ts}(\phi)$ and the characteristic curve of the exit valve $\psi_T(\phi)$:

$\psi_{ts} = (p_2 - p_1 - (\rho/2)(U+\delta u_1)^2)/(\rho U_T^2)$ and $\psi_T = \delta p_2/(\rho U_T^2)$.

Then, we can show that

$L_u + 1/\cos^2\beta_2* = -(1/\phi)(d\psi_{ts}/d\phi)$ and $R\phi = d\psi_T/d\phi$

and Eq.(16) can be expressed by:

$$\left[1+\frac{1}{\cos^2\beta_2*}\frac{l}{L}\right]B^2\phi^2\frac{d^2}{dt^2}\left(\frac{\delta u_1}{U}\right)+\left[\frac{1+(1/\cos\beta_2*)(l/L)}{(d\psi_T/d\phi)/\phi}-B^2\phi\frac{d\psi_{ts}}{d\phi}\right]\frac{d}{dt}\left(\frac{\delta u_1}{U}\right)$$

$$+\left[1-\frac{d\psi_{ts}/d\phi}{d\psi_T/d\phi}\right]\left(\frac{\delta u_1}{U}\right)=0 \tag{16'}$$

Equation (16) and (16') are the same as the equation of motion of a mass supported by a spring and a damper. Two types of instability are known to occur: static and dynamic instabilities.

The static instability occurs when the stiffness of the system (the coefficient of the third term) is negative. This occurs when

$$\frac{d\psi_{ts}}{d\phi} > \frac{d\psi_T}{d\phi} \tag{18}$$

and the operating point diverges exponentially with time from the balancing point. This suggests that the operating point is statically unstable. This is equivalent to the divergence of a wing or the buckling of a strut subjected to axial compression.

The dynamic instability occurs when the damping coefficient (the coefficient on the second term) is negative and the amplitude of vibration increases exponentially with time. This is "surge" and the onset condition can be expressed as

$$\frac{d\psi_{ts}}{d\phi} > \frac{1+(1/\cos\beta_2^*)(l/L)}{B^2(d\psi_T/d\phi)} \tag{19}$$

This shows that the surge occurs more easily when the B-factor $B=\sqrt{\rho C/L}\,U_T$ ($C=A/\rho g f$) or the resistance of the exit valve $d\psi_T/d\phi = R\phi$ is larger. We should note that a surge can occur at higher speed even in the same system where surge is not found at a lower speed, since the B-factor is proportional to the tip speed U_T. The destabilizing effect of exit valve resistance may be caused by the fact that surge is basically the oscillation of the mass of fluid in the inlet pipe with the compliance of the surge tank as the spring element. This is clearer if we consider that the frequency determined from Eq.(16') can be expressed as follows:

$$f = \frac{1}{2\pi\sqrt{\rho CL}}\sqrt{\frac{1-(d\psi_{ts}/d\phi)/(d\psi_T/d\phi)}{1+(1/\cos^2\beta_2^*)(l/L)}} \tag{20}$$

The first part ($1/(2\pi\sqrt{\rho CL})$) shows the resonant frequency of the system with the inlet pipe with the length L and the surge tank with the compliance C, and the second the effects of the rotor and the exit valve. Thus the surge frequency is basically the resonant frequency of the system and does not depend on the rotor speed.

3.0 CAVITATION SURGE

It has been shown for normal surge, that a tank or a compliant element is needed to constitute a vibration system. With cavitation, it serves as a compliant element and it is not needed to have an explicit compliant element. As the simplest model of cavitation surge, we consider a system composed of an inlet pipe with the length L, the rotor described in section 1.1, and an outlet pipe with infinite length. The last simplifying assumption suggests that there would be no flow rate fluctuation downstream of the rotor: $\delta u_2 = 0$. In addition to this, we can apply the momentum equation of the fluid in the inlet pipe, Eq.(11),

$$\delta p_1 = -\rho U \delta u_1 - \rho L(d/dt)\delta u_1 \tag{11}$$

the continuity equation across the rotor, Eq.(9) with $\partial^*/\partial t^* = \partial/\partial t$,

$$h(\delta u_2 - \delta u_1) = (\partial/\partial t)\delta V_c$$

and the cavitation characteristics of Eq.(7) with $\delta v_1 = 0$

$$\delta V_c = h^2\left[F_1\cdot(\frac{\delta u_1}{U}) + F_3\cdot(\frac{\delta p_1}{\rho U^2})\right] \quad .$$

By combining these equations, we obtain the following result.

$$\frac{d^2}{dt^2}\left(\frac{\delta u_1}{U}\right) - \frac{F_1 - F_3}{F_3(L/U)}\frac{d}{dt}\left(\frac{\delta u_1}{U}\right) - \frac{U^2}{F_3 Lh}\left(\frac{\delta u_1}{U}\right) = 0 \tag{21}$$

Since $F_3 = -2K\cos^2\bar{\beta}_1 < 0$, negative damping occurs when $F_1 - F_3 < 0$ and this leads to the onset condition of cavitation surge

$$M > 2(1+\sigma)\phi K \tag{22}$$

Equation (21) gives the cavitation surge frequency

$$f = \frac{1}{2\pi}\frac{U}{\sqrt{-F_3 Lh}} = \frac{U_T}{2\pi\sin\bar{\beta}_1}\frac{1}{\sqrt{2KLh}} = \frac{1}{2\pi}\frac{1}{\sqrt{\rho CL}} \tag{23}$$

where the last expression is obtained with $C = -F_3 h/(\rho U^2) = 2\sin^2\bar{\beta}_1 Kh/(\rho U_T^2)$. This shows that the frequency is the natural frequency of the inlet pipe-cavitation compliance system and is proportional to the impeller speed, caused by the fact that the compliance C is correlated with the tip speed. This is quite different from the frequency of normal surge (Eq.20), which is fixed to the natural frequency of the system. The above results were obtained not by using the pressure performance of the impeller (Eq.3) but by using only the continuity across the rotor (Eq.9) and the cavitation characteristics (Eq.7).

The criterion for normal surge, Eq.(19), shows that the positive slope of the pressure performance, $d\psi_{ts}/d\phi > 0$, is the cause of normal surge. If the flow rate is increased, the pressure difference across the pump is increased and this accelerates the flow through the pump. This positive feedback through the performance is the cause of normal surge. On the other hand, the criterion for cavitation surge, Eq.(22) shows that positive mass flow gain factor, $M > 0$, is the cause of cavitation surge. When the flow rate is increased, the incidence angle α_1 to the rotor blade is decreased. If $M = \partial(V_c/h)/\partial\alpha_1$ is positive, the cavity volume V_c is decreased. Then the upstream flow rate is increased to fill up the space once occupied by the cavity. This positive feed back through the continuity relation is the cause of cavitation surge. So, the mechanisms of normal surge and cavitation surge is totally different.

4.0 ROTATING STALL

For two-dimensional instabililies of rotating stall and rotating cavitation we assume that the inlet conduit length, L, is much larger than the circumferential wavelength, s, of the disturbance. A stationary frame is used for the analysis. The upstream flow disturbance produced by the flow instabilities is expressed by the following velocity potential.

$$\phi = (s/2\pi)\tilde{u}_1 \exp 2\pi j[nt - (y/s)]\exp[(2\pi/s)x] \tag{24}$$

where s, n, and j are the wavelength in the y direction, the frequency, and the imaginary unit, respectively. Real parts are considered to have physical meanings. Then the velocities u and v in the x and y directions are written as

$$u = U + \frac{\partial \phi}{\partial y} = U + \tilde{u}_1 \exp 2\pi j(nt - \frac{y}{s}) \exp(\frac{2\pi}{s} x) \tag{25}$$

$$v = \frac{\partial \phi}{\partial t} = -j\tilde{u}_1 \exp 2\pi j(nt - \frac{y}{s}) \exp(\frac{2\pi}{s} x) \tag{26}$$

where the amplitude of velocity fluctuation $\tilde{u}_1$ is assumed to be much smaller than the uniform velocity U. From the linearized momentum equation we obtain the following pressure fluctuation.

$$\delta p_1 = -\rho U(1 + jk)\tilde{u}_1 \exp 2\pi j(nt - y/s) \exp[(2\pi/s)x] \tag{27}$$

where $k \equiv sn/U$ is the reduced frequency. In general, k is complex and expressed by $k = k_R + jk_I$ and the following expression can be used.

$$\exp 2\pi j(nt - \frac{y}{s}) = \exp\left[-\frac{2\pi U}{s} k_I\right] \exp\left[\frac{2\pi j U k_R}{s}(t - \frac{y}{V_p})\right]$$

where $V_p = Uk_R = U_T(k_R / \tan\bar{\beta}_1)$ is the propagation velocity in y direction and $\tan\bar{\beta}_1 = U_T / U = 1/\phi$ with the flow coefficient ϕ. For two-dimensional disturbances shown by Eqs. (25)-(27), the time derivative in the rotating frame reduces to

$$\frac{\partial *}{\partial t *} = \frac{\partial}{\partial t} + U_T \frac{\partial}{\partial y} = 2\pi jn - U_T \frac{2\pi}{s} j = 2\pi j \frac{U}{s}(k - \tan\bar{\beta}_1)$$

The flow disturbance at the impeller inlet ($x = 0$) can be expressed from Eqs.(25) - (27) as:

$$\delta u_1 = \tilde{u}_1 \exp 2\pi j(nt - y/s), \quad \delta v_1 = -j\tilde{u}_1 \exp 2\pi j(nt - y/s) \tag{25',26'}$$

$$\delta p_1 = -\rho U(1 + jk)\tilde{u}_1 \exp 2\pi j(nt - y/s) \tag{27'}$$

The pressure rise across the rotor is given by Eq.(3). The continuity equation that neglects the effect of cavitation is

$$\delta u_2 = \delta u_1 \tag{28}$$

For the sake of simplicity, it is assumed that the flow from the impeller is delivered from the rotor to a reservoir in which the pressure is constant.

$$\delta p_2 = 0 \tag{29}$$

Substituting Eqs.(25')-(29) into the pressure rise equation (3), we obtain

$$\left[\left\{1 - L_u - \frac{1}{\cos^2 \beta_2 *} - \frac{2\pi j}{\cos\beta *}\frac{l}{s}(k - \tan\bar{\beta}_1)\right\} - 1 - jk + j(\tan\bar{\beta}_1 + L_v)\right]\frac{\delta u_1}{U} = 0 \tag{30}$$

In order that we have non-trivial solution the term in [ ] should equal to zero. This gives the characteristic equation in terms of k. Substituting $k = k_R + jk_I$, we obtain the following relations from the real and imaginary parts of the characteristic equation:

$$k_I = \frac{L_u + 1/\cos^2\beta_2^*}{1+2\pi l/(s\cos\beta^*)} = -\frac{\partial\psi_{ts}/\partial\phi}{1+2\pi l/(s\cos\beta^*)}\frac{1}{\phi} \tag{31}$$

$$\frac{V_p}{U_T} = \frac{k_R}{\tan\overline{\beta}_1} = 1 - \frac{2\zeta_s(1-\phi/\phi^*)}{1+2\pi l/(s\cos\beta^*)} \tag{32}$$

Because k_I is the damping rate of the disturbance, the onset condition of rotating stall is given by

$$\frac{\partial\psi_{ts}}{\partial\phi} > 0 \tag{33}$$

Equation (33) states that rotating stall occurs if the curve of the pressure rise in the rotor (calculated using the outlet static pressure and inlet total pressure) has a positive slope. This result is precisely the conventional one described by Greitzer [7]. By comparison of Eqs.(33) and (19), it is clear that rotating stall occurs more easily than surge. Because the flow coefficient ϕ $(=\cot\overline{\beta}_1 = U/U_T)$ satisfying Eq.(33) is generally less than the incidence free flow coefficient ϕ^* $(=\cot\beta_1^*)$, Eq.(32) yields $V_p/U_T < 1$, which indicates that the stalled region rotates with an angular speed lower than that of rotor.

Note that Eqs.(32) and (33) were obtained under the assumption that the rotor discharged to a constant pressure reservoir. Alternatively, if the flow downstream were semi-infinite and two dimensional, the term $[1+(2\pi/\cos\beta^*)(l/s)]$ in Eqs.(31) and (32) would be replaced by $[2+(2\pi/\cos\beta^*)(l/s)]$. The term 1 or 2 represents the effect of inertia of the fluid in the upstream or upstean+downstream flow fields of the rotor.

5.0 ROTATING CAVITATION

As with cavitation surge, we consider the circumstances in which there are no velocity fluctuations downstream of the impeller. The characteristics of the flow upstream of the rotor are given by Eqs.(25)-(27), the cavitation characteristics by Eq.(10). By putting Eqs.(25)-(27) into Eq.(10) and assuming $\delta u_2 = 0$, we obtain the following equation.

$$\left[1+2\pi j(h/s)(k-\tan\overline{\beta}_1)\{F_1 - jF_2 - (1+jk)F_3\}\right](\delta u_1/U) = 0 \tag{34}$$

This results in a quadratic chasracteristic equation for k. From the imaginary part of Eq.(34) we obtain the onset condition of rotating cavitation:

$$M > 2(1+\sigma)\phi K \tag{35}$$

The criterion for rotating cavitation (35) is identical to Eq.(22), the onset condition of cavitation surge. The occurrence of rotating cavitation can be explained by almost the same argument as cavitation surge. For rotating cavitation, we simply need to consider the increase of flow rate at a specific circumferential location. Therefore, rotating cavitation can be considered to be a two-dimensional instability that is caused by the destabilizing effect of the positive mass flow gain factor. As with cavitation surge, rotating caviotation can occur even at a design point, independently of the flow rate and the characteristics of the rotor. This feature of rotating cavitation is quite different from that of rotating stall. From the real part of Eq.(34), we obtain the following relation:

$$(k-\tan\overline{\beta}_1)(k+F_2/F_3) = -s/(2\pi h F_3)$$

When $V_p / U_T = k / \tan\bar{\beta}_1$ and the expressions (7') for F_2 and F_3 are used, the above equation may be written in the following form:

$$(V_p / U_T - 1)\left\{ V_p / U_T + \sigma_1 + M\phi/(2K) \right\} = (s/h)(4\pi K \sin^2 \bar{\beta}_1) \tag{36}$$

From this expression, we find that Eq.(34) has the following two solutions :

$$V_p / U_T > 1 \tag{37}$$

$$V_p / U_T < -\left\{ \sigma_1 + M\phi/(2K) \right\} \tag{38}$$

Thus, rotating cavitation has two modes. One of them rotates faster than rotor and the other rotates in the opposite direction. We term these forward and backward rotating cavitation, respectively. Earlier experimental results (for example, Kamijo et al. [9]) had noted the forward-rotating cavitation phenomenon. More recently, Hashimoto et al., [10] have also observed the backward form of rotating cavitation. It has not been clarified why forward rotating cavitation is more often observed than backward mode, although the onset conditions of both modes are theoretically the same.

6.0 MUTUAL RELATION OF FLOW INSTABILITIES

6.1 Rotating Stall and Rotating Cavitation

For rotating stall we have used the conditions of $\delta u_2 = \delta u_1$ and $\delta p_2 = 0$. Corresponding relations for rotating cavitations are cavitation characteristics and $\delta u_2 = 0$. If we combine the cavitation characteristics of Eq.(10), the impeller performance of Eq.(3) and $\delta p_2 = 0$ with the inlet flow characteristics of Eqs.(25)-(27), we obtain the following characteristic equation which can express both rotating cavitation and rotating stall:

$$\left\{ \frac{1}{\cos^2 \beta_2 *} + \frac{2\pi}{\cos\beta *} \frac{l}{s}(k - \tan\bar{\beta}_1) j \right\} \times \left[1 + 2\pi j \frac{h}{s}(k - \tan\bar{\beta}_1)\{F_1 - jF_2 - (1 + jk)F_3\} \right]$$

$$+ j(k - \tan\bar{\beta}_1) - jL_v + L_u = 0 \tag{39}$$

As before, this is based on the assumption that the rotor discharges to a constant pressure reservoir. If we assume the case $\beta_2 * \to \pi/2$ or $l/s \to \infty$, Eq.(39) reduces to

$$\left[1 + 2\pi j(h/s)(k - \tan\bar{\beta}_1)\{F_1 - jF_2 - (1 + jk)F_3\} \right](\delta u_1 / U) = 0$$

which is the same as Eq.(34), the result for rotating cavitation. This can be explained as follows. The negative slope of the head-flow rate curve becomes infinite in the limit of $\beta_2 * \to \pi/2$, and the inertia of fluid in the rotor also becomes infinite in the limit $l/s \to \infty$, and as a result δu_2 tends to zero. Rotating stall is suppressed due to the condition of $\delta u_2 = \delta u_1 = 0$. When the influence of cavitation is extremely small, F_1, F_2 and F_3 approach zero. In this case Eq.(39) agrees with Eq.(30), the result for rotating stall.

When rotating stall and rotating cavitation coexist, Eq.(39) must be solved, and it is cubic in k. When it is assumed that a two-dimensional flow continues downstream of the rotor, the term $[(2\pi/\cos\beta*)(l/s)]$ should be replaced with $[1 + (2\pi/\cos\beta*)(l/s)]$ in Eq.(39):

$$\left\{\frac{1}{\cos^2\beta_2*}+(1+\frac{2\pi}{\cos\beta*}\frac{l}{s})(k-\tan\bar{\beta}_1)j\right\}\times\left[1+2\pi j\frac{h}{s}(k-\tan\bar{\beta}_1)\{F_1-jF_2-(1+jk)F_3\}\right]$$

$$+j(k-\tan\bar{\beta}_1)-jL_v+L_u=0 \qquad (39')$$

Under this condition, the following three solutions of k have been obtained (Tsujimoto et al., 1993).

$$(V_p/U_T)_1=\mathrm{Re}(k_1/\tan\bar{\beta}_1)>1$$

$$(V_p/U_T)_2=\mathrm{Re}(k_2/\tan\bar{\beta}_1)<0$$

$$(V_p/U_T)_3=\mathrm{Re}(k_3/\tan\bar{\beta}_1)<1$$

Furthermore, the following interesting features of k_1,k_2 and k_3 emerge:

- The values of k_1 and k_2 are close to those obtained by Eq.(34), that is, k_1 and k_2 represents rotating cavitation. On the other hand, k_3 is close to that from Eq.(30), showing that k_3 represents rotating stall.
- The value of k_3 depends on the flow coefficient ϕ and loss coefficients, ζ_Q and ζ_S , whereas the influence of these coefficient on k_1 and k_2 is small.
- The mass flow gain factor M and cavitation compliance K have a substantial influence on k_1 and k_2 , but not on k_3 .
- The roots, k_1,k_2 and k_3 , can coexist, amplify, and damp independently of each other, which indicates that rotating cavitation and rotating stall are independent phenomena. Most interestingly, Murai [11] observed rotating stall with cavitation (represented by k_3 root) in experiments on an axial flow pump.

This will be discussed in detail in sections 7.1 and 7.2.

6.2 Surge and Cavitation Surge

As in the preceding section, we can investigate the case of co-existence of surge and cavitation surge by replacing the relation of $\delta u_2=\delta u_1$ in the surge analysis with the cavitation characteristics Eq.(10) . Then, the characteristic equation becomes

$$\left[\frac{1}{(1/R)+B^2\phi^2 jk_L}+jk_L+L_u+\frac{1}{\cos^2\beta_2*}+\frac{1}{\cos\beta*}\frac{l}{L}jk_L\right]$$

$$\times\left[1+\frac{h}{L}jk_L\{F_1-(1+jk_L)F_3\}\right]+jk_L+L_u=0 \qquad (40)$$

When β_2* approaches $\pi/2$ or l/L becomes infinite, Eq.(40) yields Eq.(21) with $d/dt=2\pi jn=j(U/L)k_L$ for cavitation surge. When the influence of cavitation is extremely small, F_1 and F_3 are extremely small and Eq.(40) reduces to Eq.(16) for surge. Because Eq.(40) is a biquadratic

equation with real coefficients for jk_L , there are two sets of complex conjugate solutions for jk_L, that is, $a_{1,2} \pm b_{1,2} j$. Therefore, k_L is expressed as $k_L = \pm b_{1,2} - a_{1,2} j$. Since the difference of the sign on the real part $b_{1,2}$ (frequency) has no meaning for the present case, Eq.(40) represents two types of oscillations corresponding to surge and cavitation surge. It can be shown numerically that the roots of Eq.(40) are quite close to those of Eq.(16) and (21), with the values of parameters typical for inducers. One of them corresponding to surge and mainly depends on the value of ϕ but not on the value of M , and the other corresponds to cavitation surge and mainly depends on the value of M but not on the value of ϕ. This shows that surge and cavitation surge behave quite independently when they co-exist.

Table 1 shows the onset conditions and the frequency of surge, rotating stall, cavitation surge, and rotating cavitation, obtained in the present section. The results are summarized as follows:

- Surge and rotating stall are one- or two-dimensional flow instabilities caused by a positive slope of the head-flow rate performance curve.
- Cavitation surge and rotating cavitation are also one- or two-dimensional flow instabilities caused by a positive mass flow gain factor M .
- The frequency of surge depends substantially on the characteristics of the hydraulic system.
- The rotational frequency of rotating stall depends on the performance and the geometry of the rotor. It is proportional to and smaller than the rotational speed of the rotor.
- The frequencies of cavitation surge and rotating cavitation are proportional to the rotating speed of the impeller.
- The frequency of cavitation surge is the resonant frequency of the system caused by the compliance provided by cavitation.
- Rotating cavitation has two modes: One rotates faster than the rotor and the other rotates in the opposite direction to the rotor.

Table 1: Onset Condition and Frequency of Cavitation Instabilities

Instability	Onset condition	Frequency
Surge	$\frac{\partial \psi_{ts}}{\partial \phi} > \frac{1+(1/\cos\beta^*)(l/L)}{B^2 \phi R}$	$n = \frac{1}{2\pi}\frac{1}{\sqrt{\rho C L}}\sqrt{\frac{1+(1/R)\left[L_u + \left(1/\cos^2\beta_2^*\right)\right]}{[1+(1/\cos\beta^*)l/s]}}$
Rotating stall	$\frac{\partial \psi_{ts}}{\partial \phi} > 0$	$\frac{V_p}{U_T} = 1 - \frac{2\zeta_s[1-(\phi/\phi^*)]}{1+(2\pi/\cos\beta_1)l/s]} < 1$
Cavitation surge	$M > 2(1+\sigma)\phi K$	$n = \frac{U_T}{2\pi}\frac{1}{\sin\bar{\beta}_1}\frac{1}{\sqrt{2KLh}}$
Rotating cavitation	$M > 2(1+\sigma)\phi K$	$V_p/U_T > 1, \quad V_p/U_T < 0$

7.0 EXAMPLES OF ROTATING STALL AND ROTATING CAVITATION.

In order to illustrate the results more practically and to compare them with experimental results, numerical examples are shown for rotating stall and rotating cavitation. For the comparison with experiment, it is assumed that two-dimensional flow extends to downstream infinity (Tsujimoto et al., [12]). Moreover, it is assumed that the height of the two-dimensional flow channel in the downstream of the cascade is decreased

to $1/b$ of that in the upstream. However, the characteristics of rotating stall and rotating cavitation are not influenced by these additional assumptions. Numerical calculations are made for an inducer tested by Kamijo et al. [9] for which the first detailed observation of rotating cavitation has been made.

7.1 Examination of Three Roots of Eq.(39')

Figure 3 shows three roots $k^* = k/\tan\overline{\beta}_1$ of Eq.(39'), assuming two-dimensional downstream flow. The real part gives the propagation velocity ratio $k_R^* = V_p / U_T$. The values of parameters used for the calculations are shown in the figure. Here, it is defined that $\Omega_l = 2\pi(1+b)l/(2bs\cos\overline{\beta})$, $\overline{\beta} = (\beta_1^* + \beta_2^*)/2$ and $\Omega_h = 2\pi h/s$. The static performance of the inducer is shown in Fig.4, from which the values of ζ_Q and ζ_S are obtained. In this figure, ϕ^* and ψ^* are the flow and pressure coefficients normalized by using the inducer tip speed. ψ_{th}^* is the Euler's head at the mean radius, ψ_t^* is the total head and ψ_{ts}^* is the inlet total to outlet static pressure coefficient.

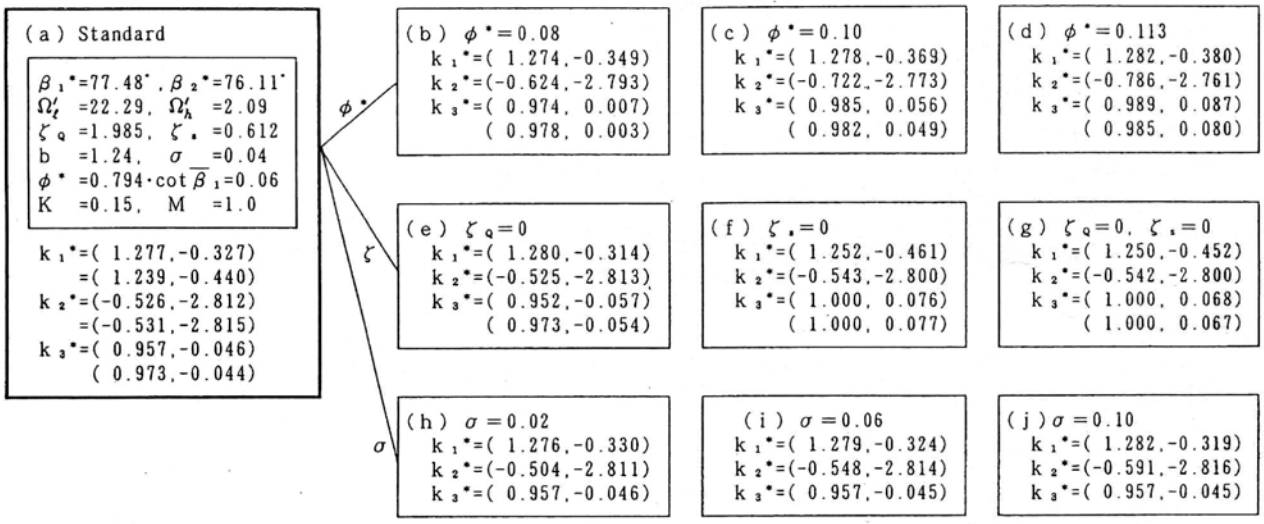

Figure 3: Three Roots of Eq.(39').

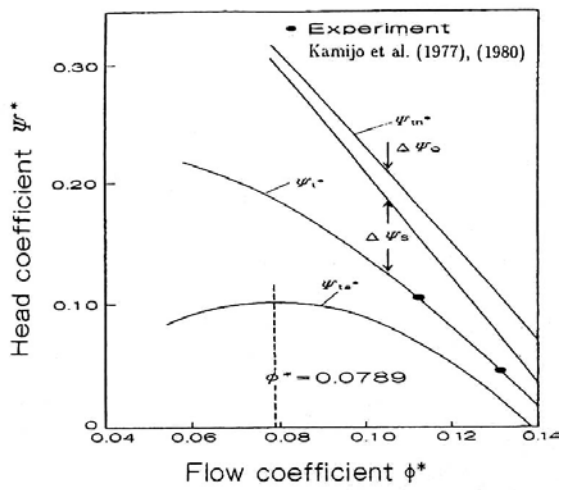

Figure 4: Static Performance of the Inducer.

Figure 3 (b)-(j) show the three roots, $k_i^* = (k_{Ri}^*, k_{Ii}^*), i = 1,3$, of the characteristic equation corresponding to Eq.(39'), with the value of parameters which is different from the standard values shown in (a). They are assigned to k_1^*, k_2^* and k_3^* following the criteria ($k_{R1}^* > 1, \quad k_{R2}^* < 0, \quad and \quad k_{R3}^* < 1$) mentioned in section 6.1. The values in the lower line of k_1^* and k_2^* in (a) are the values for the rotating cavitation obtained from Eq.(34), and the values in the lower line of k_3^* in (a)-(g) are the values for rotating stall, given by Eq.(30).

As shown in Fig. 3(a), the values of k_1^* and k_2^* are close to those obtained from Eq.(34) and k_3^* is close to those obtained from Eq.(30). This suggests that k_1^* and k_2^* represent the rotating cavitation and k_3^* the rotating stall, and that they can be approximately treated by the method outlined in sections 5.0 and 4.0, respectively. For the standard case (a), the imaginary parts of k_1^*, k_2^* and k_3^* are all negative, showing that both rotating cavitation and rotating stall can occur simultaneously. The fact that the root k_3^*, which represents rotating stall estimated under the effect of cavitation, is close to the non-cavitating rotating stall solution of Eq.(30) means that the rotating stall is not affected largely by the existence of cavitation. As shown in (b)-(g), the rotating stall is damped ($k_{I3}^* > 0$) when ϕ^* increases or ζ_S is neglected, which can be explained by Fig.4 and Eq.(33). On the other hand, the values of k_1^* and k_2^* are almost independent on the values of ϕ^*, ζ_Q, ζ_S and σ, so long as the values of M and K are kept constant. Rotating cavitations are amplified even with a negative slope of ψ_{ts}^* at larger ϕ^* or with $\zeta_S = 0$, which is quite different from the case of rotating stall.

From these numerical results, we can conclude that rotating cavitation and rotating stall are, practically, mutually independent and completely different phenomena, in the sense that their causes are different and that they behave differently, although both can be treated and deduced from the same characteristic equation (39').

Table 2 shows the relative amplitudes of the pressure and axial velocity fluctuations at the inlet and outlet of the cascade, for the case of Fig.3(a) and corresponding to $\delta p_1 / \rho U_1^2 = 1$. For each case δp_2 is much smaller than δp_1. For rotating cavitation (k_1^* and k_2^*), δu_2 is small compared with δu_1, showing that the fluctuation at the inlet is almost absorbed by the change of cavity volume. This is caused by the fact that the blade angle β_2^* is close to $\pi/2$, and supports the experimentally obtained conclusion (Kamijo et al., [9]) that "rotating cavitation is related mainly to the inlet flow conditions." On the other hand, for rotating stall (k_3^*), δu_2 is nearly equal to δu_1, with a small effect of cavity volume change. As shown above, direct effects of ϕ^* and σ on k_1^* and k_2^* are small. It has been shown that k_1^* and k_2^* are mainly dependent on M and K. Since M and K are functions of ϕ^* and σ, rotating cavitations are affected by ϕ^* and σ through M and K.

Table 2: Relative Amplitudes of Pressure and Axial Velocity Fluctuations

		$k^* = k_1^*$	$k^* = k_2^*$	$k^* = k_3^*$
$\lvert\delta p_2/\rho U_2^2\rvert$	=	(0.0591)	(0.00836)	(0.0497)
$\lvert\delta u_1/U_1\rvert$	=	(0.0563)	(0.00257)	(0.0783)
$\lvert\delta u_2/U_2\rvert$	=	(0.0129)	(0.00020)	(0.0713)

7.2 Rotating Cavitation

Contour maps of k_1* and k_2* in the M - K plane are shown in Figs.5 and 6. Values of parameters not specified in the figures are the same as those in Fig.3(a). The solid lines are obtained from the equation corresponding to Eq.(39'), while the broken lines are determined from Eq.(34). The difference between these results is small, showing that Eq.(34) simulates rotating cavitation very well. The neutral stability curve is shown by the solid line of $k_I*=0$, which is close to the criterion of Eq.(35). The rotating cavitation is amplified in the region with $k_I*<0$, under the neutral stability curve.

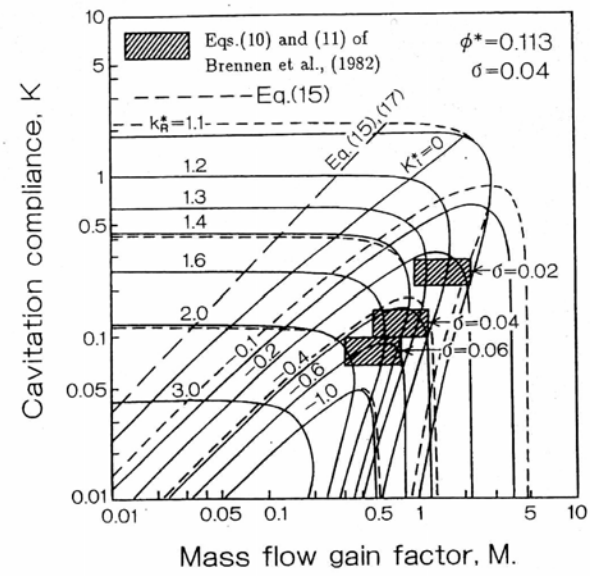

Figure 5: Contour Map of k_1^*.

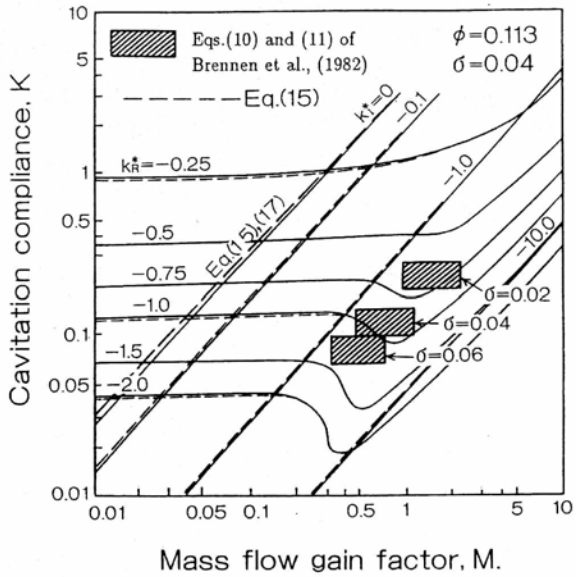

Figure 6: Contour Map of k_2^*.

In order to make comparisons with experimental results, calculations were also made for $\sigma=0.06$ and 0.02. It was found that the contour maps are almost unchanged. Hence, the ranges of M and K for three values of σ are shown in the figures, estimated from Brennen et al., [5]. For k_1* shown in Fig.5, the propagation velocity ratio for $\sigma=0.02$ is $k_R*=1.1-1.4$, which is close to the experimental value of $k_R*=1.16$ (Kamijo et al., [9]). As we reduce the cavitation number, the estimated ranges of M and K shifts to the location with smaller propagation velocity ratio k_R*. The experiments show a similar tendency. Figure 7 shows the supersynchronous shaft vibration of LE-7 LOX turbopump caused by the k_1* rotating cavitation. The reduction of the supersynchronous frequency with time is caused by the reduction of the inlet pressure with time, showing the above-mentioned tendency.

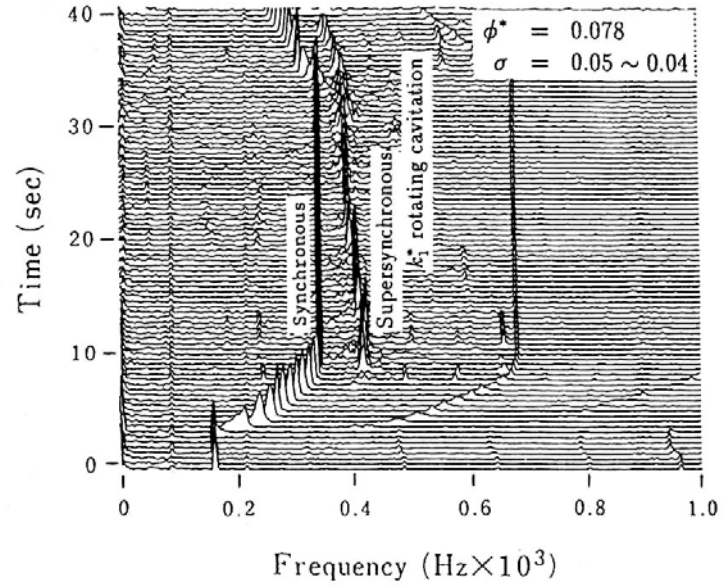

Figure 7: Supersynchronous Shaft Vibration Caused by Forward Rotating Cavitation.

Since $k_{R2}^* < 0$, the characteristic root k_2^* corresponds to a rotating cavitation which propagates in the direction opposite that of the impeller rotation. This backward rotating cavitation was found later by Hashimoto et al. [10]. The propagation velocity ratio V_p / U_T observed was –1.36 at $\sigma = 0.072$, which agrees with the result in Fig.6, $k_R^* \approx -1.25$ for $\sigma = 0.06$.

Usually, only forward rotating cavitation corresponding to k_1^* is observed and the observation of the backward rotating cavitation corresponding to k_2^* is limited to a few cases. This contradicts to the results of Figs.5 and 6, in which the amplifying rate $-k_I^*$ is much larger for the backward rotating cavitation k_2^*.

8.0 TWO-DIMENSIONAL FLOW STABILITY ANALYSIS WITH A CLOSED CAVITY MODEL

The analysis in the preceding section is basically one-dimensional and only the effect of total cavity volume fluctuation is included. The stability analysis of two-dimensional cavitating flow using a closed model of blade surface cavitation is presented in this section.

8.1 Method of Stability Analysis

We consider a cascade as shown in Fig.8 (Horiguchi et al., [13],[14]). For simplicity, we assume that the downstream conduit length is infinite and no velocity fluctuation occurs there. The upstream conduit length is assumed to be finite, L, in the x -direction and connected to a space with constant total pressure along the inlet AB.

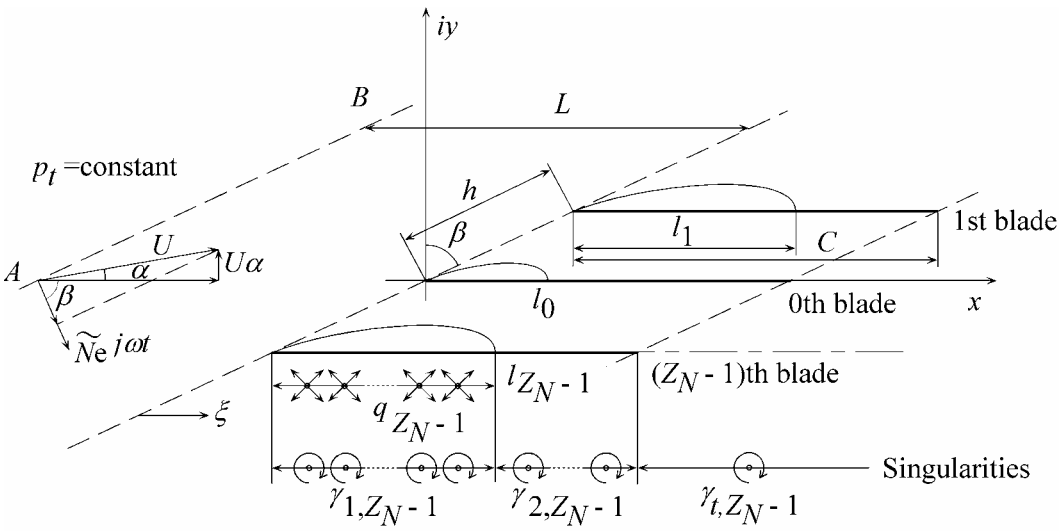

Figure 8: Cascade Geometry for Two Dimensional Cavitating Flow Stability Analysis.

We assume small disturbances with time dependence $e^{j\omega t}$ where $\omega = \omega_R + j\omega_I$ is the complex frequency with ω_R the frequency and ω_I the damping rate, to be determined from the analysis. The velocity disturbance is represented by a source distribution $q(s_1)$ on the cavity region, vortex distributions $\gamma_1(s_1)$ and $\gamma_2(s_2)$ on the blades, and the free vortex distribution $\gamma_t(\xi)$ downstream of the blades, shed from the blades associated with the blade circulation fluctuation. We divide the strength of those singularities and the cavity length into steady and unsteady components, and represent the velocity with steady uniform velocity ($U, U\alpha$), the steady disturbance (u_s, v_s), and the unsteady disturbance ($\tilde{u}, \tilde{v}$). We assume that $\alpha << 1$, $|\tilde{u}|, |\tilde{v}| << |u_s|, |v_s| << U$ and neglect higher order small terms.

The boundary conditions are:

(1) The pressure on the cavity should equal vapor pressure.

(2) The normal velocity on the wetted blade surface should vanish.

(3) The cavity should close at the (moving) cavity trailing edge (closed cavity model).

(4) The pressure difference across the blades should vanish at the blade trailing edge (Kutta's condition).

(5) Upstream and downstream conditions: the total pressure along AB is assumed to be constant and the downstream velocity fluctuation is assumed to be zero.

By specifying the strength of the singularity distributions at discrete points on the coordinates fixed to the fluctuating cavity as unknowns, the boundary conditions can be represented by a set of linear equations in terms of those unknowns. If the unknowns are separated into steady and unsteady components, the steady boundary conditions result in a set of non-homogeneous linear equations. This set of equations can be used to show that the steady cavity length l_s normalized by the blade spacing h, l_s/h is a function of $\sigma/2\alpha$.

On the other hand, the unsteady component of the boundary conditions results in a set of homogeneous linear equations. For non-trivial solutions to exist, the determinant of the coefficient matrix should be zero. This gives the characteristic equation which determines the complex frequency. Since the

coefficient matrix is a function of the steady cavity length and the complex frequency, the complex frequency $\omega = \omega_R + j\omega_I$ is determined from this relation as a function of the steady cavity length l_s / h, or equivalently of $\sigma / 2\alpha$. This shows that the frequency ω_R and the damping rate ω_I, as well as possible modes of instability, depend only on the steady cavity length l_s / h, or equivalently on $\sigma / 2\alpha$, once the geometry and other flow conditions are given. This is the most important finding of the analysis and applies also for more fundamental case of single hydrofoil.

8.2 Results of Stability Analysis

The steady cavity length obtained by assuming equal cavity on each blade is plotted in the upper part of Fig.9 (a) (Horiguti et al., [13]), for a cascade with the stagger $\beta = 80\,\text{deg}$ and the chord-pitch ratio $C/h = 2.0$, typical for turbopump inducers. In this calculation, a periodicity of disturbances over 4 blades is assumed and hence it corresponds to the case of a 4-bladed inducer. It is well known that alternate blade cavitation, in which the cavity length differs alternately, may occur for inducers with an even number of blades. The cavity lengths of alternate blade cavitation are shown in the upper part of Fig.9 (b). Alternate blade cavitation starts to develop when the cavity length, l_s, of equal cavitation exceeds 65% of the blade spacing, h.

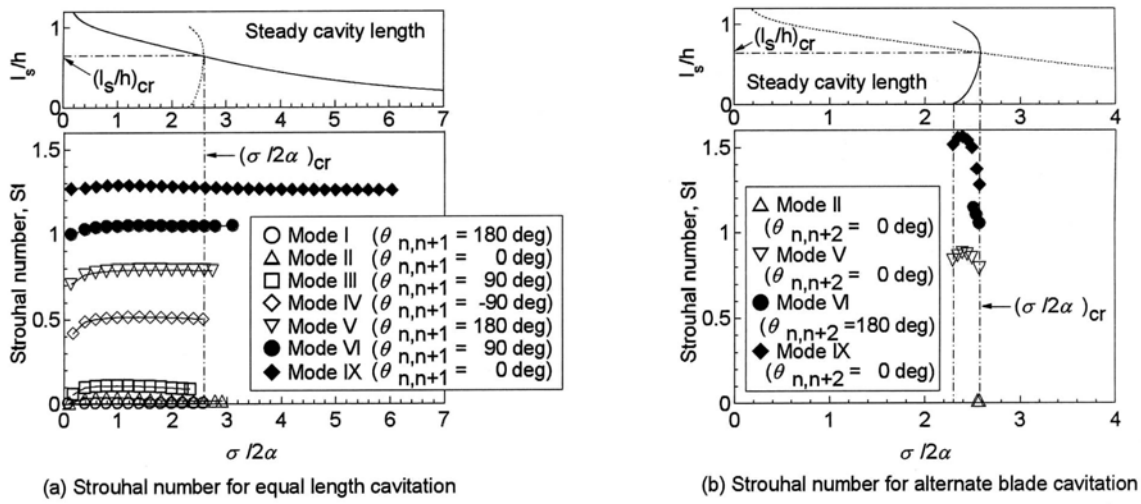

Figure 9: Steady Cavity Length (upper figures) and Strouhal Number (lower figures) of Various Modes of Cavitation Instabilities, for a 4-Bladed Inducer with the Solidity $C/h = 2.0$, Stagger $\beta = 80^o$ and the Inlet Duct Length $L/C = 1000$.

Figure 10 shows the flow field around alternate blade and equal length cavitations. Near the trailing edge of cavities, we can observe a region where the flow is inclined towards the suction surface. In this region the incidence angle to the neighboring blade on the suction side is smaller. This region starts to interact with the leading edge of the next blade when the cavity length becomes about 65% of the blade spacing. If the cavity length on one blade becomes longer than 65% of the blade spacing, the incidence angle to the next blade on the suction side becomes smaller and hence the cavity length on the next blade will decrease. This is the mechanism of the development of alternate blade cavitation.

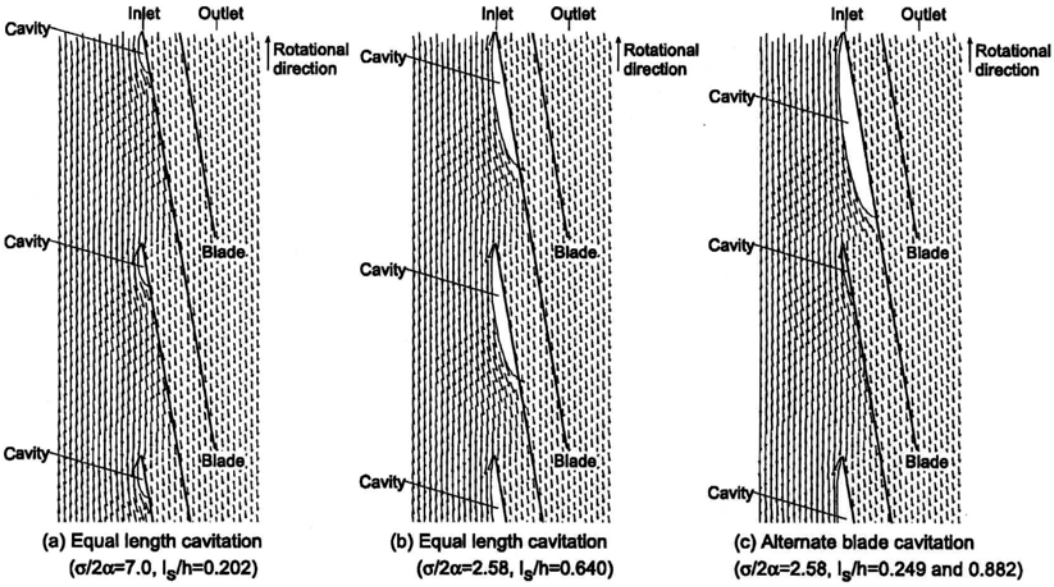

Figure 10: Alternate Blade and Equal Cavitation in a Cascade with the Solidity $C/h = 2.0$, Stagger $\beta = 80^o$ and the Inlet Duct Length $L/C = 1000$. The Incidence Angle is $\alpha = 4^o$.

Strouhal numbers $St = \omega_R l_s / 2\pi U$ of various amplifying modes are shown in the lower part of Fig.9 (a) and (b) for equal length cavitation and alternate blade cavitation. The symbol $\theta_{n,n+1}$ shows the phase advance of the disturbance on the upper blade (n+1) with respect to that on the lower blade (n) by one pitch, which is obtained as a result of the stability analysis. Here we focus on Mode I. For Mode I, the frequency is zero and the phase difference $\theta_{n,n+1}$ is 180 deg, corresponding to exponential transitions between equal and alternate blade cavitation. This mode appears for equal cavitation longer than 65% of the blade spacing, h, which shows that longer equal cavitation is statically unstable to a disturbance corresponding to the transition to alternate blade cavitation. Alternate blade cavitation does not have this mode and hence it is statically stable.

We now return to Fig.9 (a). Mode II is a surge mode oscillation without interblade phase difference: $\theta_{n,n+1} = 0$. It was found that the frequency of this mode correlates with $1/\sqrt{L}$ where L is the length of the upstream conduit. So this mode represents normal cavitation surge. Mode II is system dependent while all other modes are system independent. Mode IX is also a surge mode oscillation with no interblade phase difference but has higher frequency. This mode is herein called "higher order surge mode oscillation". Figure 11 shows the shape of cavity oscillations for these modes. The cavity volume fluctuation of Mode IX is much smaller than that of conventional cavitation surge, Mode II. For this reason the frequency does not depend on the inlet conduit length. In addition, the frequency of this mode does not depend on the geometry of the cascade and this mode occurs also for single isorated hydrofoils (Watanabe et al. [15]). This mode starts to appear at much larger values of $\sigma/2\alpha$ than other modes.

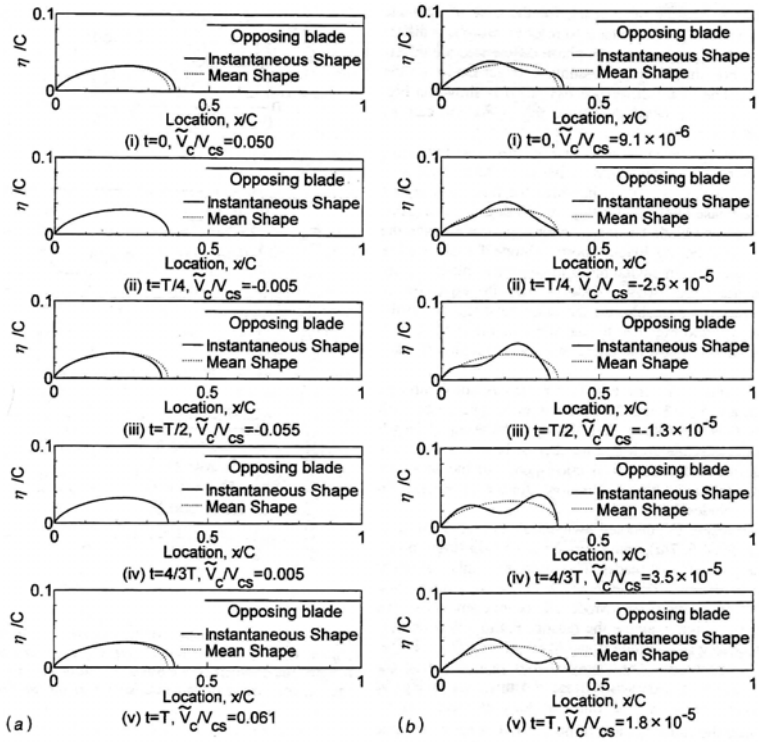

Figure 11: Oscillating Cavity Shape under (a) Cavitation Surge (Mode II) and (b) Higher Order Surge Mode Oscillation (Mode IX). $\sigma / 2\alpha = 2.0$ **and** $\alpha = 4.0^o$ **.**

Modes III-VI are various modes of rotating cavitation with various interblade phase differences. Observed from a stationary frame, the disturbance of Mode III rotates around the rotor with an angular velocity higher than the impeller speed. This is conventional rotating cavitation. Mode IV represents one-cell rotating cavitation propagating in the opposite direction of the impeller rotation and is called "backward rotating cavitation". Mode V represents 2-cell rotating cavitation. Mode VI is one-cell forward rotating cavitation with a larger propagating speed than Mode III and this mode is called "higher-order rotating cavitation". All modes except for Mode IX start to occur when the cavity length exceeds 65% of the spacing. So, those modes might be caused by the interaction of the local flow near the cavity trailing edge with the leading edge of the opposing blade, as for alternate blade cavitation. Mode IX occurs for much shorter cavities and no physical explanation has been given so far.

By the two-dimensional stability analysis, various types of higher order modes are predicted in addition to cavitation surge, forward and backward propagating modes of rotating cavitation. These higher order modes are experimentally observed less frequently compared to cavitation surge and forward rotating cavitation but they do occur (Tsujimoto et al., [16]). Since the frequencies of those higher order modes are high enough, resonance with blade bending mode vibration is possible (Tsujimoto et al., [17]). So, it is important to confirm that those instabilities are adequately suppressed by testing the inducer under all conditions encountered in real flight. It is also important to identify the reason why they occur in some cases and not in others.

Figure 12 compares the propagation velocity ratio of rotating cavitation observed in 3 and 4 bladed inducers with the results of stability analysis, plotted against the cavitation number. The propagation velocity ratio decreases as we decrease the cavitation number and it has larger values for 4-bladed inducers as compared to the case of 3-bladed inducers. These characteristics are predicted by the stability analysis. The stability limit determined from the analysis is shown in terms of cavitation number σ and

the steady cavity length l_s / h. The analysis gives much larger onset cavitation number as compared with experiments but the critical cavity length is close to $l_s / h = 0.65$. Figure 13 shows the steady cavity length at the tip and the region with rotating cavitation plotted against cavitation number, for a 3-bladed inducer. This shows that rotating cavitation occurs when the tip cavity length is larger than about 65% of the blade spacing, which agrees well with the result of 2-D cavitating flow stability analysis.

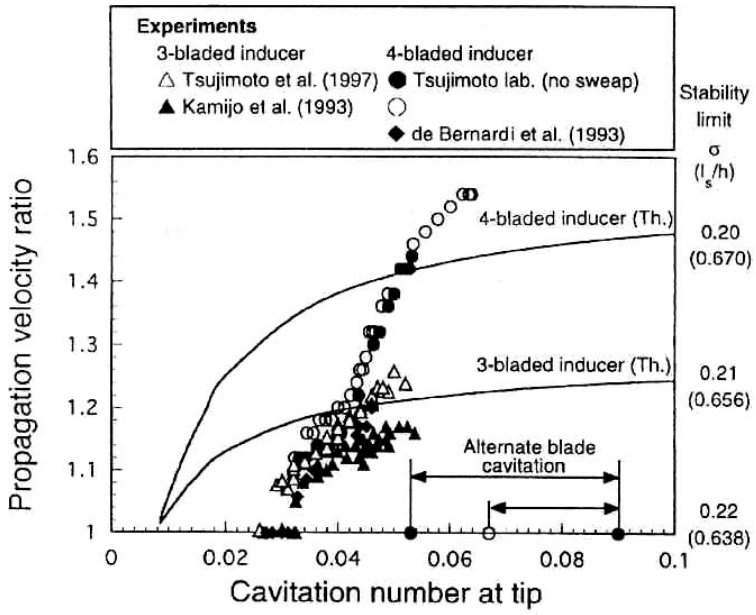

Figure 12: Propagation Velocity Ratio of Rotating Cavitation in 3- and 4-Bladed Inducers.

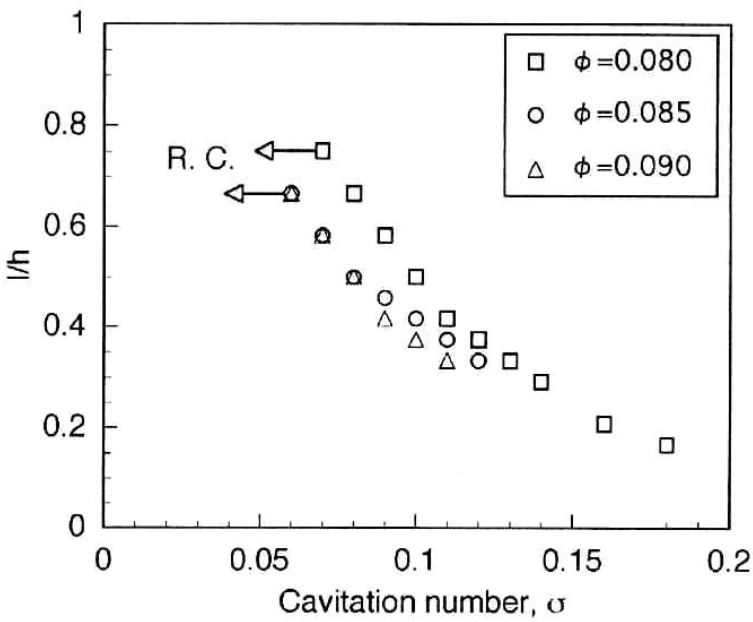

Figure 13: Cavity Length and the Region of Rotating Cavitation for a 3-Bladed Inducer.

The one-dimensional criterion $M > 2(1+\sigma)\phi K$ is satisfied under the condition $l_s = 0.65h$. So, the two-dimensional analysis gives more useful guideline for the prediction of cavitation instabilities although the one-dimensional criterion is more useful in considering the effects of various types of cavitation.

9.0 CONCLUSION

Causes and characters of non-cavitating and cavitating flow instabilities, surge, rotating stall, cavitation surge and rotating cavitation are discussed based on one dimensional stability analysis. Results of a two dimensional cavitating flow stability analysis are shown to illustrate that various modes of cavitation instabilities may occur. The results are summarized as follows.

(1) Normal surge occurs when the slope of the performance curve is larger than a certain value which is smaller when the compliance of a surge tank and the tip speed of the rotor are larger. The frequency of normal surge is basically the resonant frequency of the system composed of the inlet pipe and the surge tank and does not depend on the rotor speed.

(2) Rotating stall occurs when the performance curve has a positive slope and the stalled region rotates slower than the rotor.

(3) Cavitation surge occurs when the mass flow gain factor is larger than a certain value which is proportional to the cavitation compliance. The frequency of cavitation surge is identical to the resonance frequency of a system composed of the inlet pipe and the cavitation at the inlet of the pump. It is proportional to the rotor speed because the compliance of the cavitation is correlated with the rotor speed.

(4) The onset condition of rotating cavitation is the same as for cavitation surge. Both cavitation surge and rotating cavitation can occur even at the design flow rate and the region where the cavitation does not affect the pressure performance of the impeller. The one dimensional stability analysis predicts two modes of rotating cavitation. With one of them, the cavitated region rotates faster than the rotor (forward rotating cavitation), and with the other mode it rotates in the direction opposite to the rotor (backward rotating cavitation).

(5) A two-dimensional cavitating flow stability analysis shows that the most important parameter for the cavitation instability is the steady cavity length l_s / h or $\sigma / 2\alpha$.

(6) Various modes of cavitation instabilities including cavitation surge, forward and backward rotating cavitation and their higher order modes start to occur when the steady cavity length l_s becomes larger than 65% of the spacing h.

(7) The above condition can be easily met even at the design flow rate and without significant head decrease. So, it is required to confirm the absence of cavitation instabilities, whenever the turbomachine is required to be operated with cavitation.

An extensive review on the stability of pumping systems has been made by Greitzer [18]. It includes practical examples of rotating stall and surge as well as other types of instabilities including pressure drop and thermal instabilities. The readers are recommended to refer to this excellent article.

REFERENCES

[1] Tsujimoto,Y., Kamijo,K., and Brennen, C.E., (2001) “Unified Treatment of Flow Instabilities of Turbomachines”, *AIAA Journal of Propulsion and Power,* Vol.17, No.3, pp.636-643.

[2] Brennen, C., (1978),"The Bubbly Flow Model for the Dynamic Characteristics of Cavitating Pump," *Journal of Fluids Mechanics,* Vol.89, No.2, pp.223-240.

[3] Brennen, C.E., and Acosta, A.J., (1976),"The Dynamic Transfer Function for a Cavitating Inducer," *ASME Journal of Fluids Engineering,* Vol.98,No.2, pp.182-191.

[4] Brennen, C.E., (1994), *Hydrodynamics of Pumps*, Oxford Univ. Press and Concepts ETI, Inc., Oxord, England, U.K.

[5] Brennen, C.E., Meissner, C., Lo, E.Y., and Hoffmann, G.S., (1982), "Scale Effects in the Dynamic Transfer Functions for Cavitating Inducers," *ASME Journal of Fluids Engineering,* Vol.104, No.4, pp.428-433.

[6] Otsuka,S., Tsujimoto,Y., Kamijo,K., Furuya,O., "Frequency Dependence of Mass Flow Gain Factor and Cavitation Compliance of Cavitating Inducers", *ASME Journal of Fluids Engineering,* Vol.118, No.2, June (1996), pp.400-408.

[7] Greitzer, E.M., (1976), "Surge and Rotating Stall in Axial Flow Compressors,Part I-Theoretical Compression System Model", *ASME Journal of Engineering for Power,* Vol.98, No.2, pp.199-217.

[8] Greitzer, E.M., (1976), "Surge and Rotating Stall in Axial Flow Compressors, Part II-Experimental Results and Comparison with Theory", *ASME Journal of Engineering for Power,* Vol.98, No.2, pp.190-198.

[9] Kamijo,K., Shimura,T., and Watanabe, M.,(1977), (1980), "A visual Observation of Cavitating Inducers," *ASME Paper 77-WA/FE-14,* Nov. 1977; also *NAL Report,* TR-598T, 1980.

[10] Hashimoto,T., Yoshida,M., Watanabe, M., Kamijo,K., and Tsujimoto, Y., (1997), "Experimental Study on Rotating Cavitation of Rocker Propellant Pump Inducers," *AIAA Journal of Propulsion and Power,* Vol.13, No.4, pp.488-494.

[11] Murai, H., (1968/1969), "Observations of Cavitation and Flow Pattern in an Axial Flow Pump at Low Flow rate," *Mem. Inst. High Speed Mech.,* Vol.24, No.246,pp.315-333(in Japanese).

[12] Tsujimoto, Y., Kamijio, K. and Yoshida, Y., (1993). "A Theoretical Analysis of Rotating Cavitation in Inducers." *ASME Journal of Fluids Engineering*, Vol.115, No.1, 135-141.

[13] Horiguchi, H., Watanabe, S., and Tsujimoto, Y., (2000). "A Linear Stability Analysis of Cavitation in a Finite Blade Count Impeller." *ASME Journal of Fluids Engineering*, Vol.122, No.4, 798-805.

[14] Horiguchi,H., Watanabe, S., Tsujimoto, Y., and Aoki,M., (2000). "Theoretical analysis of Alternate Blade Cavitation in Inducers." *ASME Journal of Fluids Engineering*, Vol.122, No.1, 156-163.

[15] Watanabe, S., Tsujimoto, Y., Franc, J.P., and Michel, J.M.,(1988). "Linear Analysis of Cavitation Instabilities.", *Proc. Third International Symposium on Cavitation, April,* Grenoble, France, 347-352.

[16] Tsujimoto,Y., Horiguchi, H., and Fujii, A., (2004), "Non-Standard Cavitation Instabilities in Inducers," *Proceedings of the 10th International Symposium on Heat Transfer and Dynamics of Rotating Machinery,* March 7-11, Honolulu, Hawaii.

[17] Tsujimoto, Y., and Semenov, Y., (2002), "New Types of Cavitation Instabilities in Inducers," *Proceedings of the 4th International Symposium on Launcher Technology,* 3-6 December, Liege, Belgium.

[18] Greitzer, E. M., (1081). "The Stability of Pumping Systems-The 1980 Freeman Scholor Lecture", *ASME Journal of Fluids Engineering*, Vol.103, No.2, 193-242.